The Thesis Committee for Vikraman Parthiban
Certifies that this is the approved version of the following thesis:

Using Complex Light Modulation for Holographic Applications

APPROVED BY
SUPERVISING COMMITTEE:

Michael F. Becker, Supervisor

Alan C. Bovik

Using Complex Light Modulation for Holographic Applications

by

Vikraman Parthiban, B.A.; B.S.E.E

Thesis

Presented to the Faculty of the Graduate School of

The University of Texas at Austin

in Partial Fulfillment

of the Requirements

for the Degree of

Master of Science in Engineering

The University of Texas at Austin

May 2016

For all my friends and family,

Acknowledgements

I have seen and worked with many professors through my college career, but Mike Becker is someone I specifically would like to acknowledge because he made a significant influence in helping me decide whether to enter graduate school. I was always afraid of pursuing academia, but Mike understood and made the process seem less intimidating and trusted me like a fellow colleague. He knew how to mentor students and support them. There are many talented researchers I have met in my career, but they unfortunately lack the ability to meet students where they are at. Dr. Becker is both an intelligent individual and a wonderful advisor. He is a great person to have around especially as a friend and mentor.

Abstract

Using Complex Light Modulation for Holographic Applications

Vikraman Parthiban, M.S.E.

The University of Texas at Austin, 2016

Supervisor: Michael F. Becker

Complex light modulation is the ability to control a light-wave's phase and amplitude, thereby allowing complete control of the light-wave at any spatial location. The applied optics group at The University of Texas at Austin Electrical and Computer Engineering Department created a fully complex hologram by a combination of spatial light modulators. A digital micromirror device (DMD) was used to produce a precise amplitude profile, and a liquid crystal spatial light modulator (SLM) was used to produce the phase profile. A band-limited 4-f imaging system imaged the DMD onto the SLM to create a fully complex modulated wavefront, which reconstructed a holographic image at the desired location. With this capability, it is possible to create improved imaging methods for the consumer, medical, and defense industries as well as applications in holography. Our previous research has successfully created phase-only holograms (POH), amplitude-only beam-shaping patterns, and published simulation results on full-complex modulation. This thesis provides an in-depth experimental analysis of the full-complex hologram.

Table of Contents

List of Tables

List of Figures

Chapter 1: Introduction

In June 2011, a technology news and information website published a science article for controlling light in a novel way. Researchers at the University of Twente created a method[1] to send images through an opaque system such as a sugar cube or a glass of milk. Shown in Fig 1.1, the technique relied on controlling both the phase and amplitude components of the light wave. If harmless light can be wave-guided and refocused using the phase and amplitude, then doctors have an alternative solution to X-ray based imaging methods, which otherwise cause radiation. The technology may also be able to refocus the light inside the tissue, which enables the non-invasive photo-thermal therapy with high resolution.

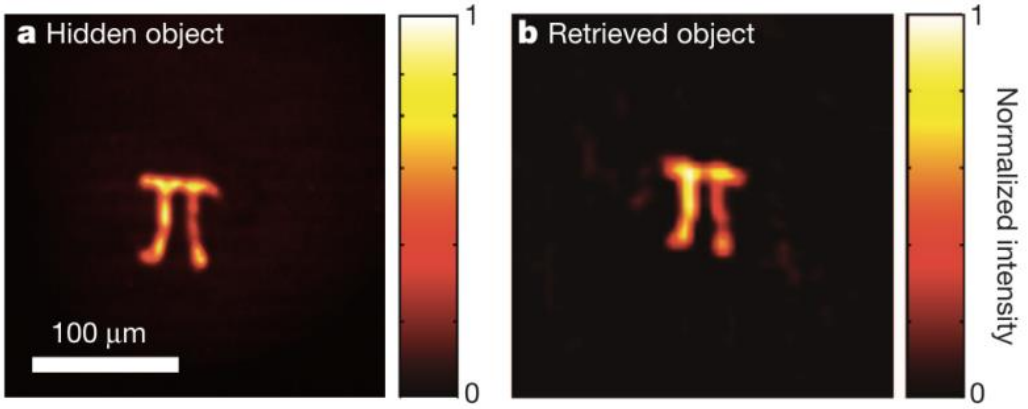

Figure 1.1: Focusing light through scattering media. (a) object hidden inside media, (b) retrieved image using phase and amplitude technique. Courtesy of Vellekoop and Mosk.

Complex light modulation (CLM) is the ability to control a light-wave's phase and amplitude, thereby allowing complete control of the light-wave at any spatial

[1] I. M. Vellekoop and A. P. Mosk, "Focusing coherent light through opaque strongly scattering media," Opt. Lett.32, 2309-2311 (2007).

location. Controlling both the phase and amplitude of light has been one of the Holy Grails of optics, and there are several applications for this technology. The applied optics group at The University of Texas at Austin Electrical and Computer Engineering Department created a fully-complex hologram (also known as Fresnel hologram) by utilizing both phase and amplitude spatial light modulators (SLMs). Most current holograms are phase-only. Our method may be beneficial for applications requiring precise wavefront reconstruction, such as biomedical imaging in tissue and three-dimensional holographic displays.

In Chapter 1, we first share the goals of this thesis and then provide a brief overview of full complex holograms and spatial light modulators. Chapter 2 delves into the theory behind scalar diffraction and how it is mathematically utilized to create backwards diffraction calculations for hologram reconstruction. Chapter 3 details our specific full-complex method and describes the SLMs we used to produce holograms. Chapters 4 and 5 discuss our hologram image quality as well as explain potential applications.

1.1 IMPORTANCE OF THIS STUDY

The field of holography has been growing rapidly over the past decade. With the advance of augmented reality and virtual reality technologies, people want technologies that can add value to worlds they live in ways where it becomes easier to perceive and manipulate the environment. Bringing holograms into the real world provides larger amounts of data in a more visualized and understandable context. Imagine if we can view a 3D hologram of CAD models from our cell phone or tablet. The next app might be a live hologram feed of an NBA game displayed on top of your phone. Complex light modulation is just one step towards realizing this potential. Crafting light waves to take

any form, hence the term "beam shaping," gives the ability to shape light for imaging applications, such as medical therapy, security algorithms, and of course consumer 3D holo-displays.

This thesis examines the experimental results of a complex light modulation technique introduced and simulated by Liang and Becker[2] in 2014. The goal was to utilize high precision amplitude beam shaping developed by Liang, et. al[3] and pair the technology with off-the-shelf liquid crystal (LC) phase modulation technology to create a high quality hologram. These efforts depended on the results of digital micromirror device (DMD) characterization for beam shaping as well as phase modulation using LC technology. In this thesis, we first provide some background and theory for full complex modulation, describe various full-complex modulation techniques, and share an overview of SLM technology. Afterwards we progress to show how a DMD was used to create the amplitude portion of the hologram and how the LC modulator was used to create the phase portion of the hologram. In conclusion, we provide an image analysis of each hologram produced and compare the full complex results with phase-only and iterative phase-only hologram designs.

1.2 HISTORICAL REVIEW OF FULL-COMPLEX HOLOGRAPHY

In the early 20th century, Nobel Laureate Dennis Gabor introduced[4] the first hologram. Holograms have been vastly improved in recent years, especially with the advances of augmented reality systems like Microsoft Hololens[5] and MagicLeap[6], but

---

[2] Liang, J. and Becker, M. F. , “Precise holograms using complex light modulation,” Proc. of SPIE 8979, 89790D-1 to 9 (2014).
[3] Jinyang Liang, Rudolph N. Kohn, Jr., Michael F. Becker, and Daniel J. Heinzen, "High-precision laser beam shaping using a binary-amplitude spatial light modulator," Appl. Opt. 49, 1323-1330 (2010)
[4] D. Gabor, "A New Microscopic Principle", Nature, 161, 777, 1948.
[5] "Microsoft HoloLens." Microsoft HoloLens. Microsoft, n.d. Web.
[6] "Magic Leap." Magic Leap. N.p., n.d. Web.

much of the bottleneck in improving hologram reconstruction fidelity depends on the quality of spatial light modulators. Most holograms produced today are phase-only, which inherently contains less information than both amplitude and phase. In the following sections, we look at technologies where both amplitude and phase are considered.

1.2.1 Full-complex modulation with two one-parameter SLMs

In 1991, Florence and Juday[7] studied full-complex modulation by adding the "operating curves" of two SLMs. They described three fundamental methods that reduced signal-to-noise (SNR) ratios of the holographic image and provided a signal decomposition for their methods. Given the inherent restrictions of the SLMs available at this time, they explored filtering techniques, such as the full complex matched filter, and ways to collapse the full-complex data onto the coupled-parameter SLMs.

1.2.2 Full-range, continuous, complex modulation by two coupled-mode LCTVs

In 1996, researchers from Canada demonstrated[8] another full-complex technique by utilizing commercially available liquid crystal TVs obtained from the green panels of two Epson Crystal Image™ video projectors. Utilizing the electro-optic properties of the twisted-nematic LCTV, they were able to make one panel operate in the phase-mostly regime, and the second operate in the amplitude-mostly regime. By carefully aligning the two LCTVs in an afocal imaging system with a pinhole spatial filter in between, they minimized Moiré effects and grid patterns, and produced a fully complex hologram. Whereas Florence and Juday added the two modulating curves (real and imaginary) to

---

[7] James M. Florence ; Richard D. Juday; Full-complex spatial filtering with a phase mostly DMD. Proc. SPIE 1558, Wave Propagation and Scattering in Varied Media II, 487 (November 11, 1991); doi:10.1117/12.49655.

[8] Luiz Gonçalves Neto, Danny Roberge, and Yunlong Sheng, "Full-range, continuous, complex modulation by the use of two coupled-mode liquid-crystal televisions," Appl. Opt.35, 4567-4576 (1996).

demonstrate a fully-complex wavefront, Neto et. al performed the multiplication of the amplitude and phase. As shown in Equation 1, the full complex information (the z term) can be represented by either the addition of real and imaginary parts or as the multiplication of the amplitude, A, with the exponential of the phase, θ.

$$z = a + ib = Ae^{i\theta} \qquad (1.0)$$

1.2.3 Near-perfect hologram reconstruction with a SLM

In 2008, researchers from Austria[9] utilized one SLM to create a fully-complex hologram. By displaying two phase masks side-by-side on a single phase-only modulator and folding the light path to sequentially pass through both masks, the team was able to create a fully-complex modulated wavefront.

1.2.4 Precise holograms using complex light modulation

In 2014, Becker and Liang simulated[10] a full-complex technique that utilized Texas Instruments' digital micromirror device (DMD) and a liquid crystal SLM to create a fully-complex hologram. This method was unique because it uses a dedicated amplitude system that was separate from the phase modulator. The DMD functions as an amplitude modulator because of its binary pixel elements that are made up of 13.68 μm wide micro-mirrors that switch on or off independently. After applying error diffusion and low-pass filtering, this amplitude modulator was aligned carefully with the phase-only SLM to produce a fully complex modulated wavefront. This thesis examines the experimental results of applying this technique.

---

[9] Alexander Jesacher, Christian Maurer, Andreas Schwaighofer, Stefan Bernet, and Monika Ritsch-Marte, "Near-perfect hologram reconstruction with a spatial light modulator," Opt. Express 16, 2597-2603 (2008).
[10] Liang, J. and Becker, M. F. , “Precise holograms using complex light modulation,” Proc. of SPIE 8979, 89790D-1 to 9 (2014).

1.3 SPATIAL LIGHT MODULATORS

A crucial part of a holographic image or video system is the quality of the spatial light modulator (SLM) being used. Considered as the "engines" for the holographic displays, SLMs encode information onto the lightwave itself. Most state-of-the-art SLMs have several disadvantages. Some are large and bulky and others cannot handle the large data frame rates for holo-video (several holographic images per second). In Fig. 1.2, a test holographic image produced by Smalley et al.[11] is shown which was produced by a liquid crystal on silicon (LCOS) SLM. The image labeled “b” contains the desired image and the rest of the images are extraneous. Such extraneous images are typical for holographic image systems based on pixilated SLMs such as liquid crystals (LC) and MEMS devices.

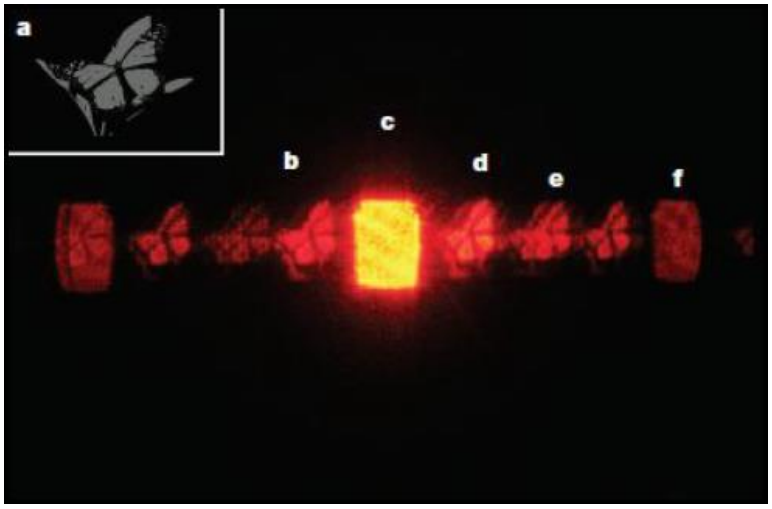

Figure 1.2: Artifacts from holographic stereogram based on a LCOS SLM. (a) stereogram mask, (b) intended output, (c) zero-order spot, (d) conjugate images. Courtesy of MIT Media Lab.

[11] D.E. Smalley, Q.Y.J Smithwick, V.M. Bove Jr., J. Barabas, and S. Jolly. Anisotropic leaky mode modulator for holographic video displays. Nature 498. June, 2013.

Other typical limitations of SLMs for holographic display include low bandwidth (unable to handle large amounts of data quickly), high cost, low diffraction angle (producing small viewing angles), and poor scalability. In liquid crystal and MEMS devices, pixel densities are already highly optimized and yet current pixel densities do not lend themselves well to large diffraction angles, which translates to small viewing fields in displays. Smalley et al. claims that a typical LC SLM system is limited to an output angle of just 2.54 degrees, whereas their custom acousto-optic modulator can do 24.7 degrees. Some groups have been able to extend the viewing angle of pixilated systems, but it is at the cost of incorporating multiple expensive, bulky SLMs into the system.

Table 1.1 compares different spatial light modulators used for holographic image and video displays. All of these SLMs are phase-only, and they are compared with regards to speed, pixel count, viewing angle, and cost.

	QinetiQ[12]	**Univ. of Arizona[13]**	**MIT Media Lab[14]**
Phase SLM type	Liquid Crystal	Photorefractive	Acousto-Optic
Speed	Video Rate	Still Images	Video Rate
Pixel Count	24 Gpix	-	1.7 Gpix
Viewing Angle	-	52 deg	25 deg
Cost	>$1000	-	$500

Table 1.1: Phase SLM comparison

[12] C. Slinger, C. Cameron, and M. Stanley. Computer-Generated Holography as a Generic Display Technology. IEEE. 2005.
[13] P.A. Blanche, et al. An Updatable Holographic Display for 3D Visualization. Journal of Display Technology, 4. 2008.
[14] D.E. Smalley, Q.Y.J Smithwick, V.M. Bove Jr., J. Barabas, and S. Jolly. Anisotropic leaky mode modulator for holographic video displays. Nature 498. June, 2013.

To attempt to solve problems associated with the traditional SLMs, MIT built their own SLM technology based on anistropic leaky-mode couplers, which rely on acousto-optic transducers to modulate light instead of liquid crystal or photorefractive material.

1.3.1 Digital Micromirror Device

In the previous section, we saw that all of the SLMs shown modulate the phase of light only. The Digital Micromirror Device (DMD) is a special type of SLM that modulates the amplitude of light. Traditionally, the DMD functioned primarily as part of the Texas Instruments DLP projection systems used in modern theaters around the world. However, many researchers have found this tiny chip essential in many beam shaping and holography applications. Made up of two million individually controlled micromirrors, each 13.6 μm in pitch, the DMD can modulate light at high-speed video rates. Chapter 3 will describe in detail how the DMD works in conjunction with a phase-only LC SLM to produce the full-complex hologram.

The theory behind using these SLMs to create complex hologram is to be described in the following chapter.

Chapter 2: Theory

In this chapter, we explore the theory behind creating a hologram. Before going any further, it is important to make the distinction between the word "hologram" and "reconstructed image." In the previous chapter, these words were synonymous to each other, but in the subsequent chapters, "hologram" refers to the diffractive pattern stored on the spatial light modulator, and "reconstructed image" refers to the replicated image in space.

2.1 Rayleigh-Sommerfield diffraction

Before an image is reconstructed in space, the original image properties must be stored on the diffracted lightwave. To replicate the light waves bending around our target image, we need to understand the diffractive nature of light. Diffraction, simply put, is the bending of light waves as they interact at an edge. For example, if you shout at a corner, diffraction of the sound waves makes it possible to hear around the corner. The Rayleigh-Sommerfield diffraction theory quantifies the bending of light waves mathematically. This theory hinges on solving the basic diffraction problem that requires finding a solution to the time-dependent wave equation, shown below, for a propagating wave encountering a planar screen (in our case our target image).

$$\nabla^2 U(\mathbf{r}, t) = \frac{1}{c^2} \frac{\partial^2 U(\mathbf{r}, t)}{\partial t^2}$$

∇^2 is the Laplacian operator, $U(\mathbf{r}, t)$ represents the wave under study, and c is the speed of light. Since we are interested in the time-independent spatial solution, we can use separation of variables on $U(\mathbf{r}, t)$, which becomes $U(\mathbf{r})T(t)$. Substituting this result into

the wave equation followed by simplification and rearranging of terms, we obtain the Helmholtz equation, shown below.

$$(\nabla^2 + k^2)U(\mathrm{x},\mathrm{y},\mathrm{z}) = 0 \quad where\ k = \frac{\omega}{c} = \frac{2\pi}{\lambda}$$

This form of the wave equation makes it mathematically easier to solve our diffraction problem. *U*(x,y,z) is a scalar and describes the amplitude and phase of the wave, which is what we are solving for. To match the effect of a diffracting screen on the z = 0 plane, we impose boundary conditions on this solution:

$$U(\mathrm{x},\mathrm{y},0) = U_o(\mathrm{x},\mathrm{y},0) \qquad \text{inside aperture}$$
$$U(\mathrm{x},\mathrm{y},0) = 0 \qquad \text{outside aperture}$$

U_o describes the incident wave. The well-known Rayleigh-Sommerfield diffraction integral for *U* at a distance *z* behind an aperture in a planar mask is

$$U_{RS}(x',y',z) = -\frac{i}{\lambda}\int_{Area} U_o(x,y,0)\frac{e^{ikr}}{r}cos\chi dxdy$$

where $r = \sqrt{(x'-x)^2 + (y'-y)^2 + z^2}$ is the distance between (x,y,0) and (x',y',z). χ is the diffraction angle at point (x,y,0).

2.2 FOURIER REPRESENTATION AND BACKWARDS DIFFRACTION

The diffraction integral in section 2.1 can also be written in Fourier terms with spatial frequency components. This is useful for generating amplitude and phase patterns quickly from software tools, such as MATLAB.

$$U(x', y', z) = \frac{e^{ikz}}{i\lambda z} e^{i\frac{\pi}{\lambda z}(x^2+y^2)} \mathcal{F}\left\{U(\xi, \eta, 0) e^{i\frac{\pi}{\lambda z}(\xi^2+\eta^2)}\right\}$$

where the spatial amplitude is given by $U(\xi, \eta)$, and $\Im\{\}$ represents the Fast Fourier Transform. The spatial frequency variables are denoted by $f_x = \frac{x}{\lambda z}$ and $f_y = \frac{y}{\lambda z}$. To design our hologram, we must "backwards diffract" to the source target image. This can be done by simply taking the inverse of the Fourier integral as shown here:

$$U(\xi, \eta) = (-i\lambda z)\, e^{ikz} e^{i\frac{\pi}{\lambda z}(\xi^2+\eta^2)} \mathcal{F}^{-1}\left\{U(x, y) e^{i\frac{\pi}{\lambda z}(x^2+y^2)}\right\} \text{ for } z < 0$$

where $\mathcal{F}^{-1}\{\}$ represents the inverse Fourier transform, and the spatial frequency variables are denoted by $f_\xi = \frac{\xi}{\lambda z}$ and $f_\eta = \frac{\eta}{\lambda z}$. We can easily compute the FFT and its inverse in MATLAB to do forward and backwards propagation for the hologram.

2.3 RECONSTRUCTION DISTANCE

Using the information from sections 2.1 and 2.2, we can finally derive an efficient "backwards propagating" algorithm from the image. Now, we need to know where the reconstructed image will be produced spatially. The reconstruction distance is designed to be some multiple of $z_{critical}$, where $z_{critical}$, is given by

$$z_c = \frac{M_o \Delta_o^2}{\lambda}$$

where $2z_c$ is the closest distance at which all pixels can diffract to all locations on the reconstructed image. M_o stands for pixel number (across the hologram, 512 in our case). λ is the wavelength of the illuminating light (in our case 633nm HeNe laser). Δ_o is the pixel pitch of the spatial light modulator being used (in our case the LC SLM with 15 μm

pixel pitch). As we create the hologram, we must take care to not truncate any high spatial frequency elements (parts of image that contain important data) and prevent aliasing.

2.4 SPATIO-TEMPORAL BANDWIDTH

Spatial bandwidth determines the quality of the hologram. Since this study focuses on static holographic images, temporal bandwidth is not studied in depth. There are three main issues that affect spatial bandwidth when utilizing the aforementioned backwards light propagation algorithm. First, we must consider the finite size of both the SLM and the target image (image to be reconstructed). Second, the backwards diffracted light to the SLM is often smaller than that on the target image. Third, we must avoid truncating light at the edges of the SLM to not lose important information.

To solve the issue of bandwidth, we can pad our original image by a factor of two. As shown in Fig. 2.1, the window is M x M pixels wide at both the hologram and reconstruction image planes (in our case being 1024 x 1024). The hologram is M_o pixels wide and the reconstructed image is M_w and they are related by $M = M_w = 2M_o$. The reconstruction distance, z, is expressed as a multiple of z_c; and thus $z = z_f z_{fc}$. The bandwidth of the target image can then be limited by utilizing a 4th order Butterworth infinite impulse response filter[15], the reason for which is described in further detail in the hologram design routine in Section 3.2.5. We can verify the hologram design methods by simulating forward propagation back to the target plane and evaluating the error from the original target image.

[15] Liang, J. and Becker, M. F., "Precise holograms using complex light modulation," Proc. of SPIE 8979, 89790D-1 to 9 (2014).

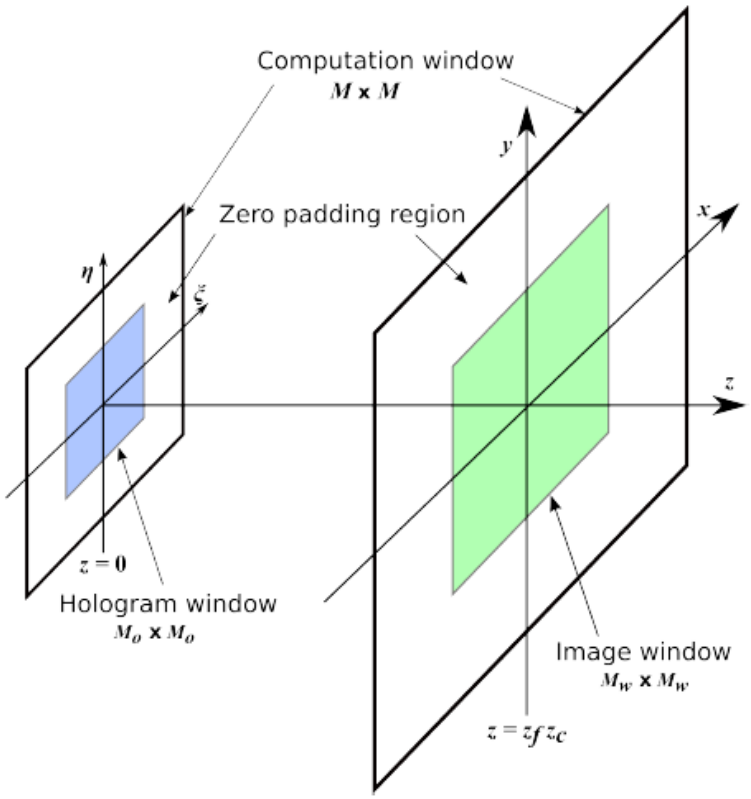

Figure 2.1: Relationship from hologram plane (ξ, η) at z = 0 to reconstructed image plane (x,y) at z = $z_f z_c$.

The experimental implementation of these techniques to create the complex hologram is to be described in the following chapter.

Chapter 3: Experiment

Our experimental implementation of fully complex light modulation is summarized as follows. We first compute the amplitude and phase profiles of the hologram using a backward diffraction calculation from the desired target image. Shown in Fig. 3.1, a digital micromirror device (DMD) is used to produce the hologram amplitude profile, and a liquid crystal spatial light modulator (SLM) displays the phase profile. A band-limited 4-f imaging system images the DMD onto the SLM to generate a fully complex wavefront that reconstructs a holographic image at the desired location. During the experiments, adjustments were made to optimize the design of the amplitude pattern via error diffusion and low pass filtering, and to carefully align and scale the amplitude pattern onto the phase SLM. The reconstructed images were further analyzed for image quality with respect to the target image.

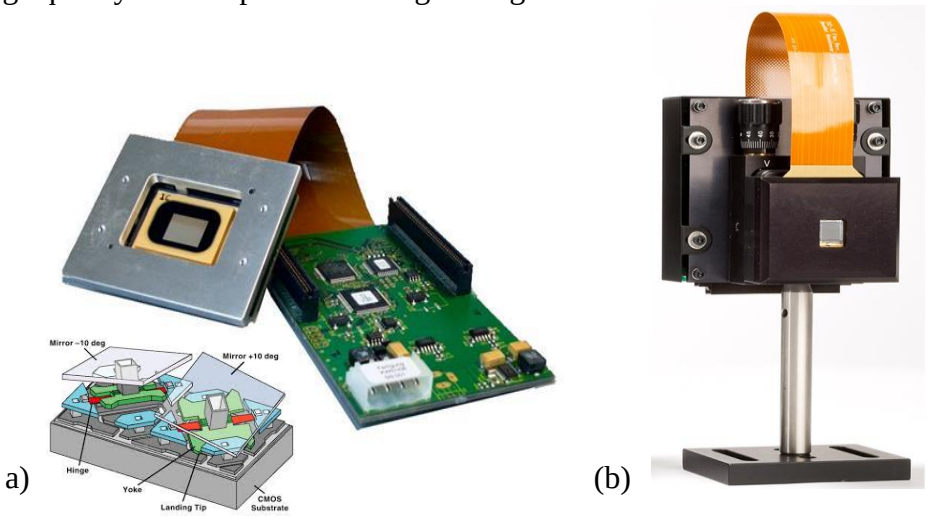

Figure 3.1: Spatial Light Modulators, (a) DMD Discovery 1100 manufactured by Texas Instruments, and (b) Reflective Phase SLM manufactured Meadowlark Optics (now Boulder Nonlinear Systems).

3.1 OPTICAL SETUP

The optical setup used to reconstruct a fully complex wavefront is shown in Fig. 3.2. After expansion and collimation, a quasi-Gaussian, 633 nm HeNe laser beam is incident on the DMD Discovery 1100, which is a 1024 x 768 pixel array with a 13.68 μm pixel pitch. The DMD pattern, designed by the error diffusion algorithm[16], is projected to the image plane by a two-lens telescope consisting of f1 and f2, both of which are 500 mm focal length lenses. The telescope magnification is thus unity, and small size adjustments to this image are made by resizing the pattern on the DMD. A pinhole low-pass filter controls the system bandwidth and filters out all high spatial-frequency noise introduced by binary spatial amplitude modulation of the DMD. As a result, the binary DMD pattern is converted to a continuous grayscale image of the desired hologram amplitude.

An SLM is placed at the image plane of the band-limited 4-f imaging system. The phase pattern is produced by a Meadowlark Optics XY-series liquid crystal spatial light modulator (Model P512-532), which is a 512 x 512 pixel array with a 15 μm pixel pitch. Using a lookup table calibrated for 633nm, this phase-only modulator is capable of displaying 1000-8000 levels of phase with a DVI 16-bit controller.

The fully complex Fresnel hologram is reconstructed at distance of 364 mm from the phase SLM ($2*z_c$ for the experimental conditions). The reconstructed image is captured by a Point-Gray Grasshopper Express CCD camera (Model GX-FW-10K3M-C), which is a 1024 x 1024 pixel array with a 5.5 μm pixel pitch. The camera was set to have a linear gamma and 14-bit digitized grayscale images were recorded without saturation of critical image data.

[16] Liang, J. and Becker, M. F., "Precise holograms using complex light modulation," Proc. of SPIE 8979, 89790D-1 to 9 (2014).

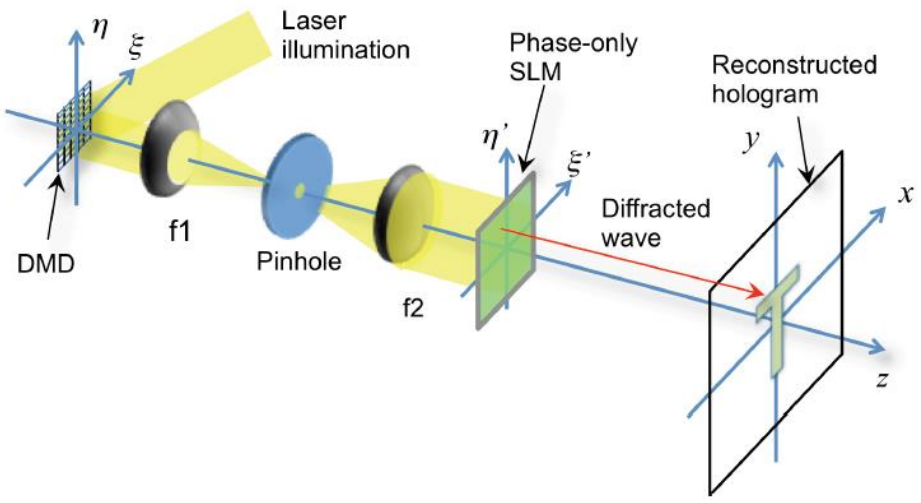

Figure 3.2: Optical setup to produce a complex wavefront and reconstruct a Fresnel hologram.

3.2 HOLOGRAM IMPLEMENTATION ROUTINE

In order to create the fully complex hologram, five steps were required:

1. Compute the desired amplitude and phase patterns from backward diffraction
2. Obtain optical system calibration images (Gaussian input beam, size calibration pattern, dark field camera image)
3. Rescale amplitude hologram pattern to match the phase SLM
4. Compute the desired DMD reflectance function, design the bit pattern using error diffusion, and compute spatial filter size for minimum RMS error
5. Align the two patterns at the phase SLM face.

3.2.1 Amplitude and Phase pattern calculation

To begin the process, the complex hologram was computed using the backward diffraction algorithm described by Liang and Becker[17]. Briefly explained mathematically

[17] Liang, J. and Becker, M. F., "Precise holograms using complex light modulation," Proc. of SPIE 8979, 89790D-1 to 9 (2014).

in Chapter 2, this technique uses the Fresnel diffraction integral expressed as a single Fourier transform of the source function, multiplied by the phase kernel for backward propagation,

$$U(x,y)\phi(x,y) = U_R(x,y)e^{-i\frac{\pi}{\lambda(z_f z_c)}(x^2+y^2)}$$

where z_f represents the dimensionless fractional propagation distance $|z|/z_c$. The target amplitude is now the real function $U_R(x,y)$. $\phi(x,y)$ represents the Fresnel phase factor. The Fourier transform becomes a digital Fourier transform (DFT) when the system is sampled. Care must be taken to eliminate aliasing and minimize errors due to truncation of high spatial frequency components in the target image as explained in sections 2.3 and 2.4.

The result of this design technique is illustrated by the following example. Complex hologram images are shown in Fig. 3.3. The target image, Fig. 3.3(a), was a 256 x 256 grayscale Lena image placed in a 512 x 512 field. The padding is required in order to limit data loss in the backward propagation computation. If the target image size and thus the corresponding phase pattern were doubled, then the SLM edge would truncate many of the fringes. The target image was also low-pass filtered with a 4th order Butterworth filter so that 90% of the image power occupied 35% of the possible bandwidth of the 512 x 512 field[18]. In other words, the image bandwidth was limited to 35% of the Nyquist frequency, f_N, of the samples. Bandwidth limiting the target image also reduced data loss of high spatial frequencies near the image edge by preventing truncation of hologram data at the SLM edge.

[18] Liang, J. and Becker, M. F., "Precise holograms using complex light modulation," Proc. of SPIE 8979, 89790D-1 to 9 (2014).

Fig. 3.3(b) and 3.3(c) represent the amplitude, $U_R(x, y)$, and phase, $\phi(x, y)$, components of the target image. As expected, the amplitude resembles the near-field diffraction pattern of a square with extra details depending on the target image. On the phase image, we see higher spatial frequencies at the edges resulting from the edges of the target image. However most of the image properties are encoded in the middle.

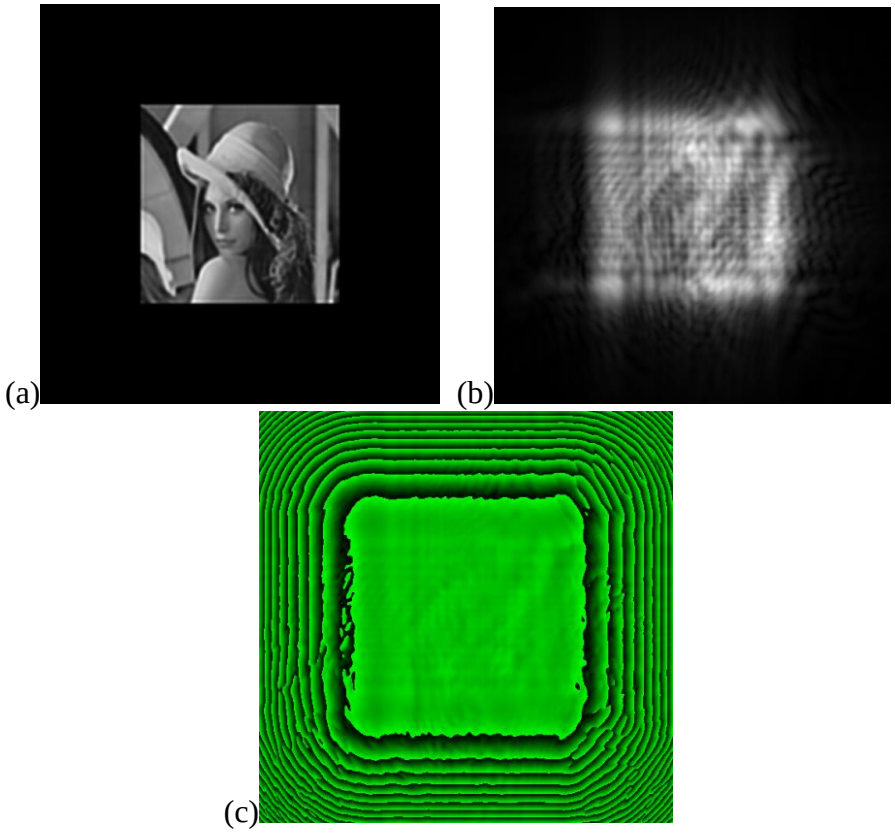

Figure 3.3: Lena hologram designed by backward propagation, (a) full 512 x 512 target image (35% bandwidth), (b) amplitude hologram pattern, and (c) phase hologram pattern.

3.2.2 Calibration

Second, the optical system had to be calibrated in order to obtain the best hologram. An additional lens (focal length = 300 mm) was used to image the phase SLM

surface onto the camera with an appropriate magnification that filled the image area. An image of the Gaussian laser beam with all of the DMD pixels set to 'ON', shown in Fig. 3.3, was used to compensate for the non-uniform input illumination of the DMD. One advantage of using this method for amplitude pattern generation is that imperfections in the illuminating laser beam amplitude can be easily compensated, and the desired pattern can be precisely generated.[19][20] In addition, an image of an array of white spots at known positions on the DMD was acquired to scale the camera image back to the DMD plane. A dark field image was also acquired and subtracted from all data images.

(a) 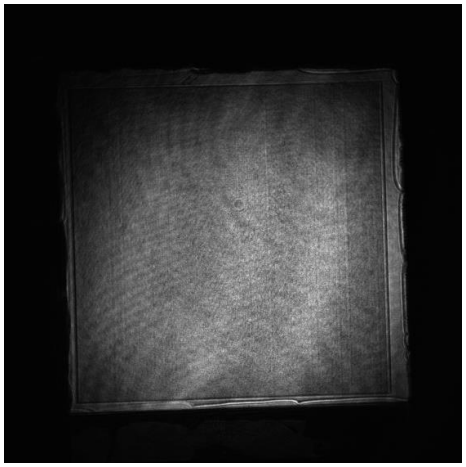 (b) 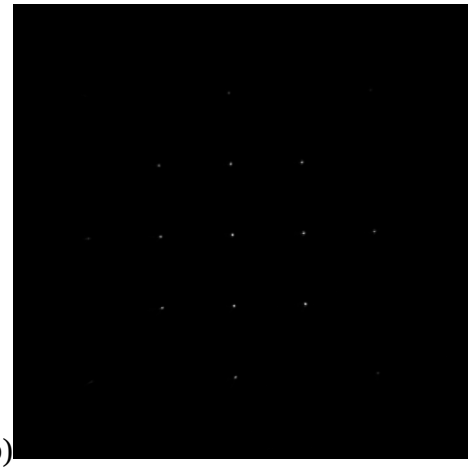

Figure 3.4: Calibration images, (a) Input quasi-Gaussian beam at the camera plane with all the DMD mirrors set to 'ON,' and (b) Array of spots to scale camera image to DMD plane.

[19] Liang, J., Kohn, R.N., Becker, M.F., and Heinzen, D.J., "1.5% root-mean-square flat-intensity laser beam formed using a binary-amplitude spatial light modulator," Applied Optics vol. 48(10), 1955-1962 (2009).

[20] Liang, J., Kohn, R.N., Becker, M.F., and Heinzen, D.J., "High-precision laser beam shaping using a binary-amplitude spatial light modulator," Applied Optics vol. 49(8), 1323-1330, (2010).

The Point Grey camera was also adjusted as shown in Fig. 3.5 to function as a linear image irradiance detector. The settings provided uniformity when comparing holograms captured by the camera during the experiment.

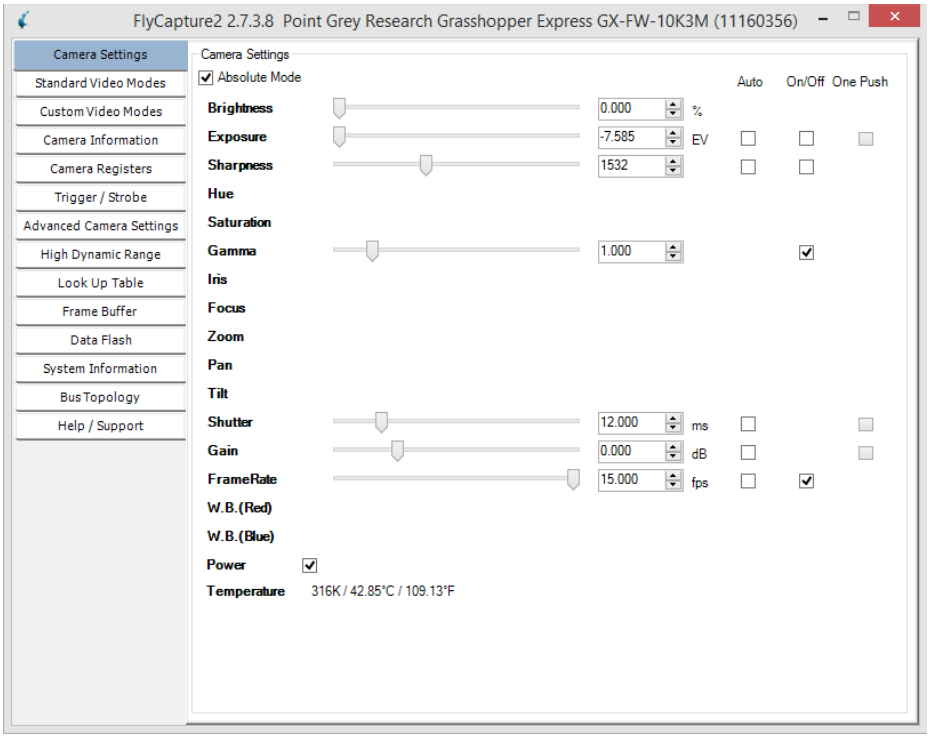

Figure 3.5: PointGrey FlyCapture camera settings.

The camera software, FlyCapture, was adjusted so that brightness set to 0%, Gamma value set to 1, and Gain set to 0. The shutter and frame rate were the only variables adjusted depending on the amount of light diffracted onto the image. Generally the brightest pixels were set to be below saturation and above half of saturation.

3.2.3 Rescale Amplitude Pattern

Third, the amplitude hologram pattern shown in Fig. 3.3(b) had to be resized to match the 512 x 512 area of the phase SLM. This was done using grid patterns on the

DMD and matching them to similar grid patterns on the SLM (while imaging the SLM face to the camera). To match the pixel width of the phase SLM, the amplitude image was scaled from 512 x 512 to 552 x 552 pixels at the DMD. Then, this pattern was loaded into the DMD after padding with black pixels to 1024 x 768 (the size of the DMD). The bits outside of the 552 pixel square region were turned off to avoid imaging outside of the phase SLM active area. Several patterns were generated in which the size was stepped above and below 552 pixels to check that this was indeed the optimum size that matched the SLM size.

3.2.4 Compute reflectance function and error diffusion

Fourth, the DMD reflectance function was obtained by the ratio of the scaled amplitude pattern to the measured input quasi-Gaussian beam profile, shown in Fig. 3.6. This was an important part of the procedure because it determines the light intensity diffracted from the DMD amplitude pattern onto the SLM.

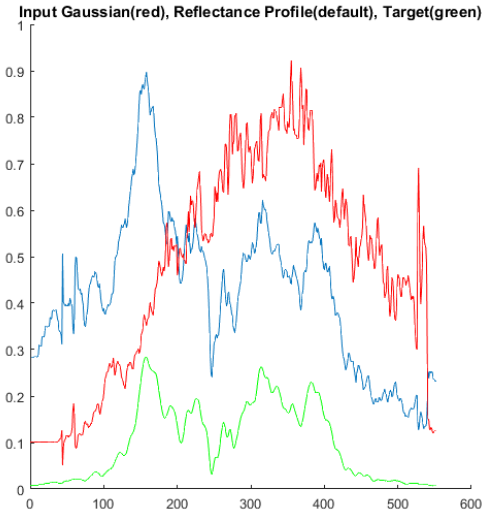

Figure 3.6: Horizontal section of the reflectance profile, shown in blue.

The green curve represents a horizontal slice from a scaled amplitude pattern (also termed as target image), the red curve represents a horizontal slice of the input Gaussian profile from Fig. 3.4(a), and the calculated DMD reflectance function is the green curve divided by the red curve, shown in blue.

This continuous reflectance function was then converted to the binary DMD pattern using the Ostromoukhov error diffusion algorithm[21]. The computed output amplitude pattern was then scaled and subtracted from the initial pattern to get the error image. The DMD pattern was further refined by adaptively turning on or off individual pixels to minimize the computed error image[22][23] shown in Fig. 3.7. This iterative refinement is based only on numerical diffraction to the reconstructed image. For this work, we did not use the further step of iterative refinement based on a captured reconstructed image.

[21] Ostromoukhov,V., "A simple and efficient error-diffusion algorithm," Proc. SIGGRAPH 2001, pp. 567–572, ACM, New York, NY (2001).
[22] Liang, J., Kohn, R.N., Becker, M.F., and Heinzen, D.J., "1.5% root-mean-square flat-intensity laser beam formed using a binary-amplitude spatial light modulator," Applied Optics vol. 48(10), 1955-1962 (2009).
[23] Liang, J., Kohn, R.N., Becker, M.F., and Heinzen, D.J., "High-precision laser beam shaping using a binary-amplitude spatial light modulator," Applied Optics vol. 49(8), 1323-1330, (2010).

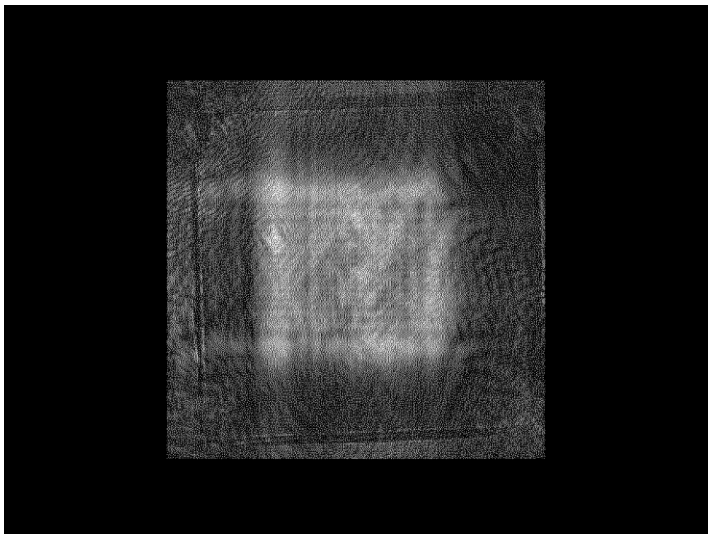

Figure 3.7: DMD pixel pattern designed from the amplitude hologram using error diffusion, scaling, and padding to 1024 x 768.

3.2.5 Spatial filtering

Low-pass filtering the amplitude hologram removed any high frequency content originating from the binary nature of the DMD pixels and the blue noise resulting from the error diffusion algorithm. For grayscale images, Liang et al.[24] found that the RMS error in the image was correlated with the optical system bandwidth. To keep the RMS error of the amplitude pattern below 10%, a system bandwidth of 35% (of the DMD modulator maximum spatial bandwidth or Nyquist frequency) was used.

The optical bandwidth of the spatial pinhole filter was adjusted to match the desired bandwidth of the amplitude pattern. The design algorithm simulated several sizes of low-pass filter, and the one that produced the lowest RMS error for the image was selected.

[24] Liang, J., Wu, S.-Y., Kohn Jr, R. N., Becker, M. F., and Heinzen, D. J., "Grayscale laser image formation using a programmable binary mask," Optical Engineering, 51(10), (2012).

3.2.6 Align DMD and Phase SLM

Finally, in order to replicate the hologram correctly, the DMD and SLM images needed to be correctly aligned (in scale, rotation, and translation) and flipped correctly with respect to each other. We used a checkerboard amplitude pattern, shown in Fig. 3.8, to align with a checkerboard phase pattern to finalize the optical alignment.

(a) 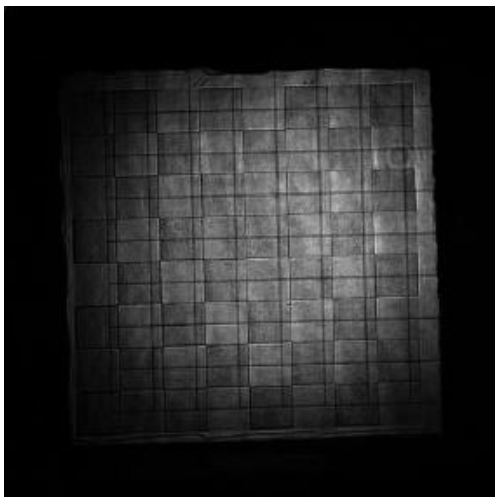 (b) 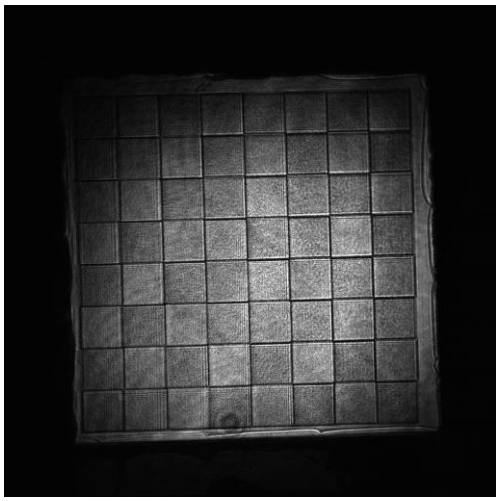

Figure 3.8: Grid alignment, (a) improperly aligned, and (b) correctly aligned.

With this optical setup finally calibrated and aligned, we can now make some test holograms. Starting from designing amplitude and phase patterns to low-pass filtering techniques, this setup procedure was repeated for every trial. The experimental holograms are analyzed in the Chapter 4.

Chapter 4: Results and Discussion

4.1 Spatial Frequency Resolution

Since the spatial frequency content of the target image was carefully chosen to be one that could be reproduced by the system, the frequency response of the reconstructed image was measured first. The test image was a 256 x 256 binary Air Force resolution chart, shown in Fig. 4.1(a). The red box, shown in Fig. 4.1(b), is selected for analyzing spatial frequencies near the bandwidth limit (bar patterns of 28%, 31%, 35% and 40% of f_N, the Nyquist frequency).

(a) 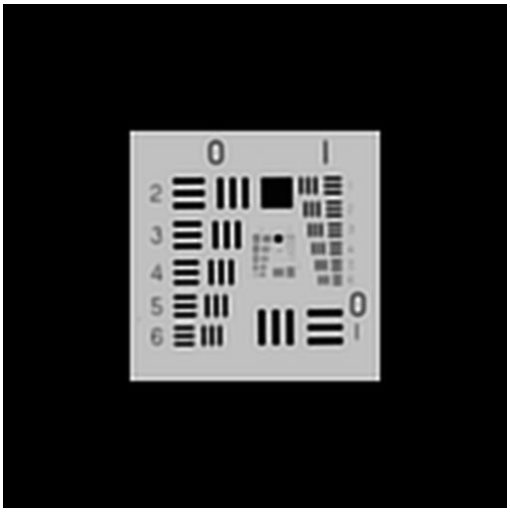 (b) 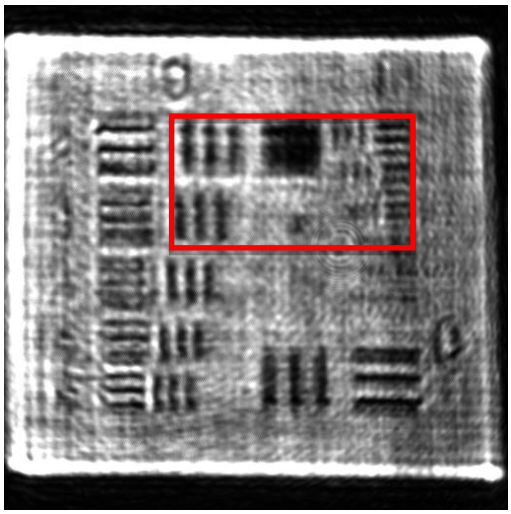

Figure 4.1: (a) Full 512 x 512 Air Force resolution chart target image (35% bandwidth), (b) reconstructed image (white level adjusted).

Fig. 4.2 expands the red box region for the target and reconstructed images respectively. In Fig. 4.2(a), the filtered target image is shown to just resolve 35% as expected. Figure 4.2(b) shows that horizontal frequencies extend to 35%, and vertical frequencies extend to 31% at this particular image distance. In addition, as can be seen in Fig. 4.2(b), the reconstructed holograms showed an 11.5% reduction in height.

These last two observations point to the effect of astigmatism of the DMD surface, shown in Fig. 4.2(c), on the reconstructed images. Both the reduction in reconstructed image height and the difference in horizontal and vertical spatial frequency longitudinal positions of the focused image arise from this astigmatism. The effect was directly visible when setting the pinhole longitudinal location in the telescope. There were distinctly different vertical and horizontal best-focus positions. The pinhole was set midway between the two, where the beam was approximately circular.

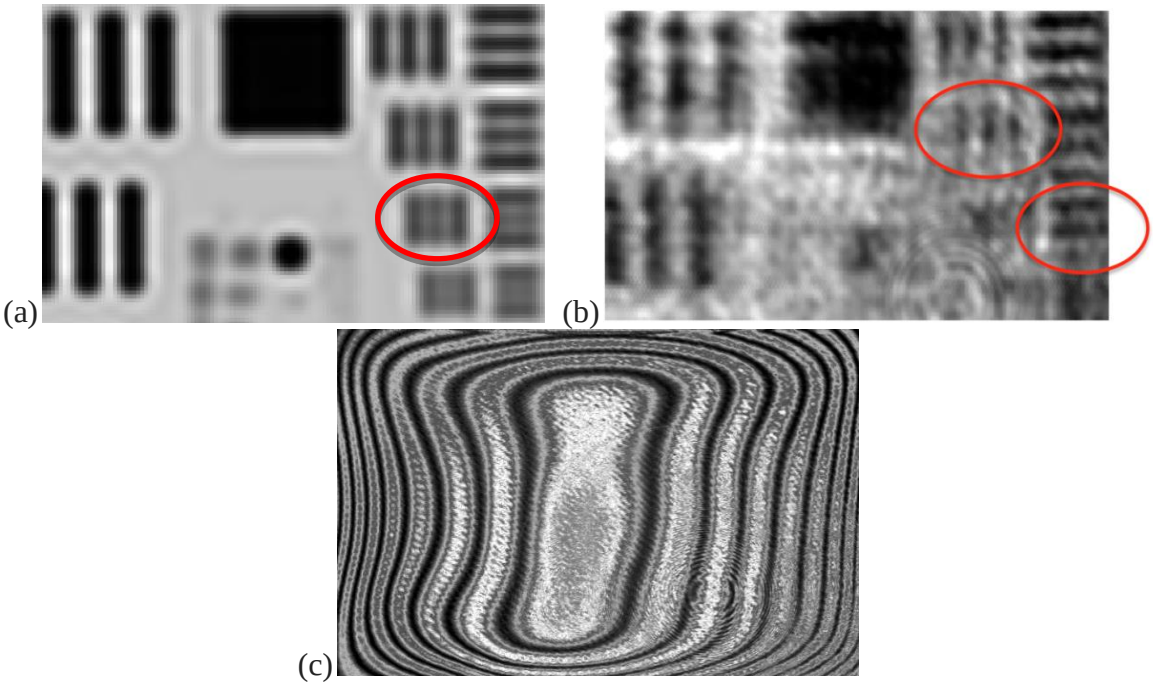

Figure 4.2: (a) Target Image; red circle f = 0.35 * $f_{N,}$ (b) reconstructed image; upper left circle, f = 0.31* f_N, lower right circle, f = 0.35* $f_{N,}$ and (c) interference phase contour of the DMD surface (1024 x 768) at 633 nm wavelength.

4.2 GRADIENT BARS

To measure grayscale mapping to the reconstructed image, a 256 x 256 grayscale gradient bars image, shown in Fig. 4.3(a), was used. As with all the target images, it was filtered to 35% of f_N. In the reconstructed image, the gradient bars image was not uniformly well reproduced, as seen in Fig. 4.3(b).

(a) 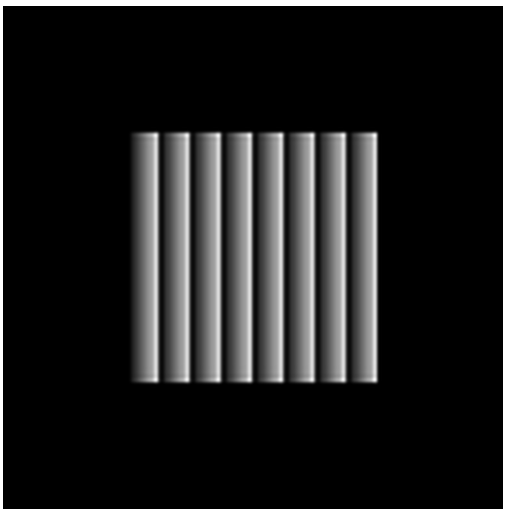 (b) 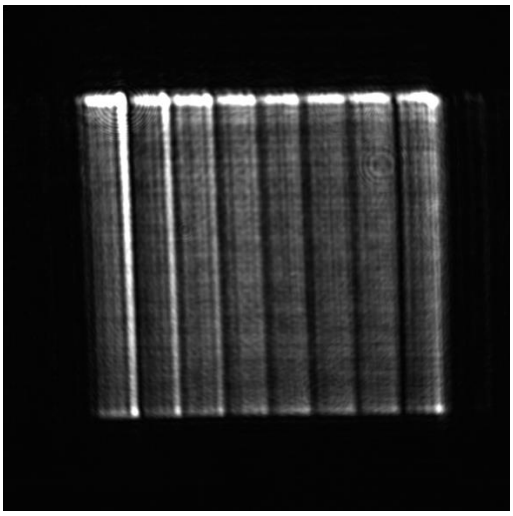

Figure 4.3: (a) Target image, low pass filtered, and (b) reconstructed holographic image.

A horizontal slice through the reconstructed image was taken to examine the gradient mapping properties as shown in Fig. 4.4. Mapping of the quasi-linear target image gray level profile to the reconstructed image was variable depending on location in the image. Fig. 4.4 shows the variability by regions with some good and some not so good reproduction of the grayscale gradient. This gray level distortion should be less evident when reconstructing high-contrast target images.

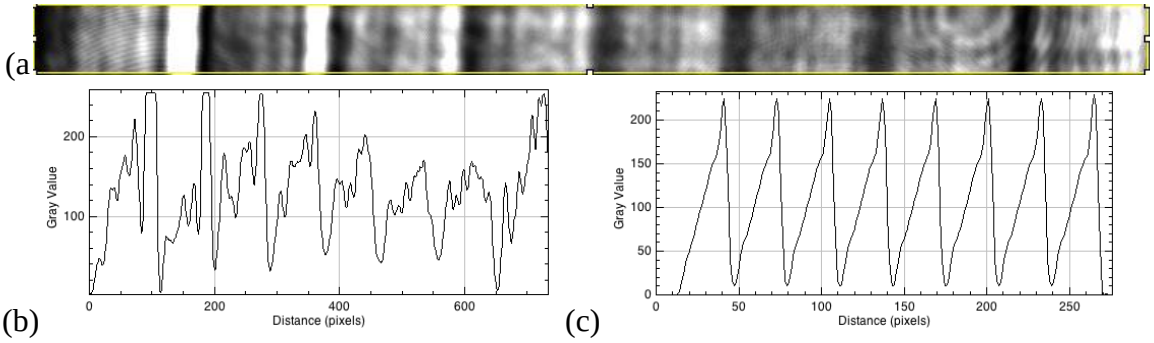

Figure 4.4: (a) Hologram reconstruction section to analyze (white level adjusted), (b) gray level plot of section analyzed, and (c) gray level plot of the target image (low pass filtered).

4.3 CAMERAMAN GREYSCALE TARGET IMAGE

The third target image was a 256 x 256 grayscale cameraman with large filled regions and high contrast. The target and holographic reconstructed images are shown in Fig. 4.5. The high contrast of the target image with areas separated by a large difference in gray level gave a better hologram reconstruction. The solid areas were appropriately filled in, and fine details were present (confirming the frequency response measurement), but the grayscale mapping was not good in some regions. Lower contrast regions (e.g., on the horizon) lost visibility. This included the tower and buildings located behind the cameraman. Added noise or artifacts included a cloth-weave pattern over entire reconstructed image, and some regions showing edge enhancement at sharp, high-contrast edges. Much like the grayscale bars image, this added edge enhancement at high-contrast edges was location dependent.

(a)  (b) 

Figure 4.5: (a) Target image (256 x 256 cropped section low pass filtered), and (b) reconstructed fully complex hologram (white level adjusted and 11.5% vertical expansion).

4.4 LENA GREYSCALE TARGET IMAGE

The last image tested was a 256 x 256 grayscale Lena that had much finer gradations in contrast (in addition to a few sharply contrasted edges). The target image is shown in Fig. 4.6(a) and the fully complex hologram reconstructed image is shown in Fig. 4.6(b). As observed for the cameraman, a broad range of gray levels was not properly reproduced in the reconstructed image, and edge enhancement can be clearly seen at the top and sides of the hologram. The cloth wave pattern is also visible across the image.

(a)  (b) 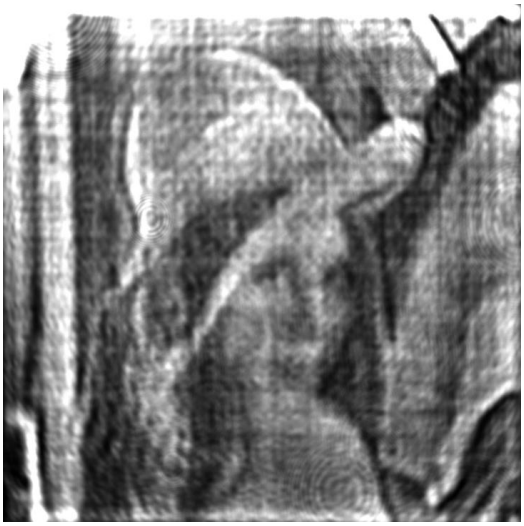

Figure 4.6: (a) Target image (256 x 256 cropped section low pass filtered), and (b) reconstructed fully complex hologram (white level adjusted and 11.5% vertical expansion).

4.5 COMPARISON TO PHASE-ONLY HOLOGRAMS

The fully complex Lena hologram was compared with a phase-only hologram and an iterative Gerchberg-Saxton generated hologram,[25] shown in Fig. 4.7. The phase-only image is shown in Fig. 4.7(a-b), and the iterative result is shown in Figure 4.7(c). Compared to the full complex image in Fig. 4.6(b), the phase-only image reveals only a general contour of the target image. Considerably less light is diffracted to the reconstructed target image, while much light is diffracted to the sharp features, particularly at the image edges. This is a direct result of the uniform illumination of the phase hologram resulting in increased light diffracting from the fringes distributed widely over the hologram by the sharp edges in the target image. This produces edge-enhancement in the reconstructed image. Furthermore, the weave pattern is brighter relative to the reconstructed image as can be seen in the brightened version in Fig. 4.7(b).

[25] Gerchberg, R.W. and Saxton, W.O., "A practical algorithm for the de- termination of the phase from image and diffraction plane pictures," Optik 35, 237–246 (1972).

Simulation of hologram reconstruction that included the dead space of the phase-only SLM revealed an identical weave pattern in the reconstruction. The weave pattern is attributed the zero-order diffraction (ZOD) from the SLM dead space. It is in effect the Fresnel diffraction of the square SLM aperture filled with the dead space between the pixels.

(a) (b)

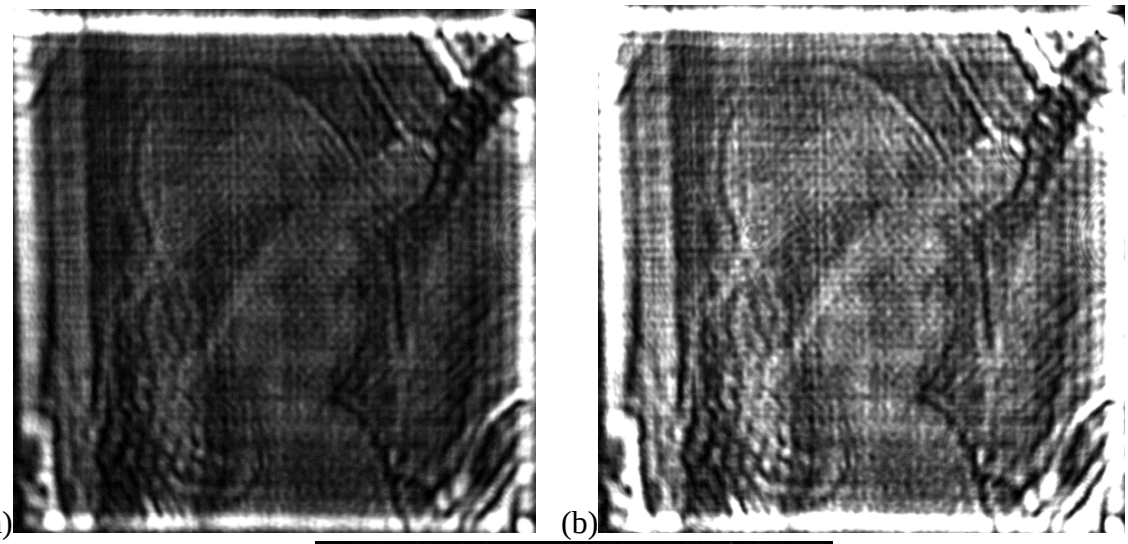

(c)

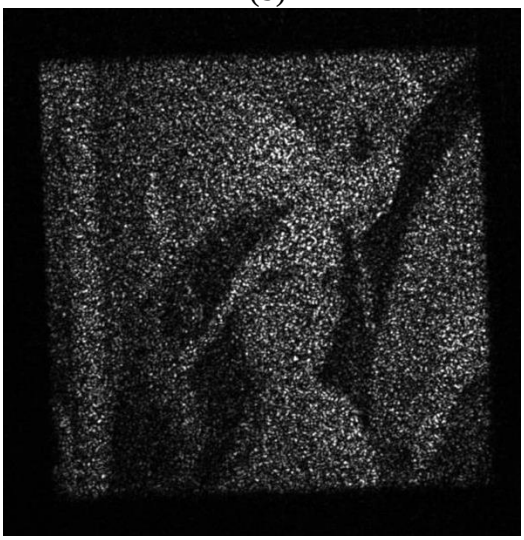

Figure 4.7: Comparison with other hologram creation methods. (a) Phase-only encoding, (b) same as (a) but white level adjusted to show detail of face, and (c) iterative Fresnel transform encoding.

The full complex image was also compared to the phase only iterative G-S algorithm in Fig. 4.7(c). The G-S method introduces a considerable amount of speckle noise as expected, but the general contour of the target image was still visible with reasonable sharpness and gray-scale rendering. Low-pass filtering reduces some of the speckle, and there is no weave pattern visible here.

Fig. 4.8 shows a reconstructed image of the cameraman hologram generated using the Gerchberg-Saxton iterative routine. Similar to the Fig. 4.7(c) with Lena, this image contains much speckle. The large contrast of the target image allowed the cameraman outline to reconstruct in the Fresnel plane, but fine details are obscured by the speckle noise.

(a) 

Figure 4.8: Cameraman reconstruction from iterative Fresnel transform encoding (G-S algorithm) hologram.

4.6 ADDITIONAL HOLOGRAMS

In addition to the previous images shown, we did several experimental iterations using additional binary and greyscale images from our digital image library. All of the target images analyzed were 256 x 256 to fit the SLM after padding.

4.6.1 Binary Bevo Bat

Out of curiosity, we wanted to test how well the SLM could beam shape the laser light into two small binary bat and bevo images located diagonally opposite from each other. Shown in Fig. 4.9, it is clearly obvious that the bat was not shaded as well, and the bevo hologram (our UT Longhorn mascot) did not show a black spot in the middle. The edges of the reconstruction images were quite blurred and not as fine as expected.

(a) 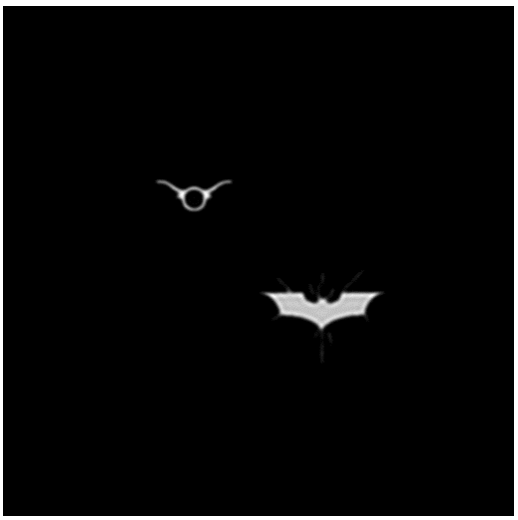 (b) 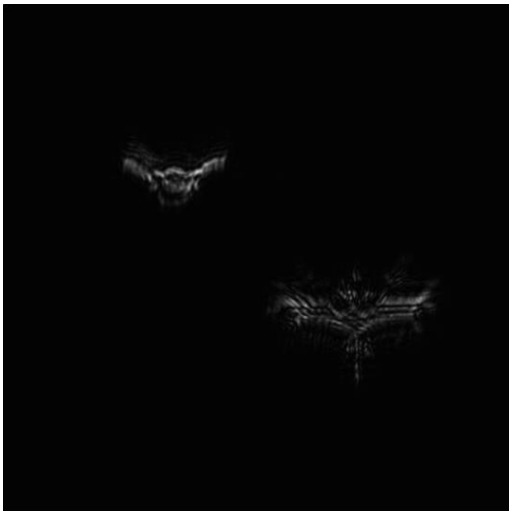

Figure 4.9: (a) Bevo Bat Target 256 x 256 image, low pass filtered, and (b) reconstructed holographic image.

4.6.2 Checkerboard

Another binary pattern tested was the checkerboard, as shown in Fig. 4.10. These hologram images were surprisingly well reconstructed. Though there are some fringe effects near the top, most of the image successfully reveals the black and white pattern.

(a) 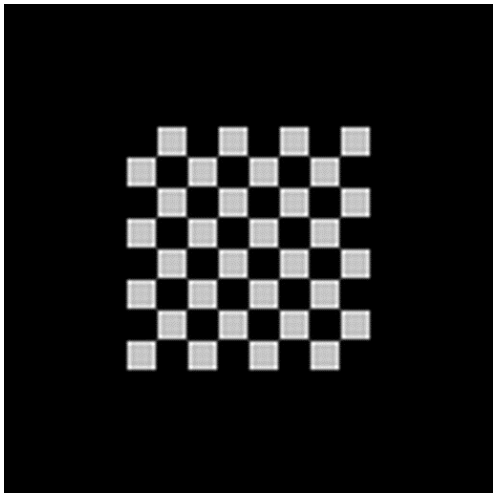 (b) 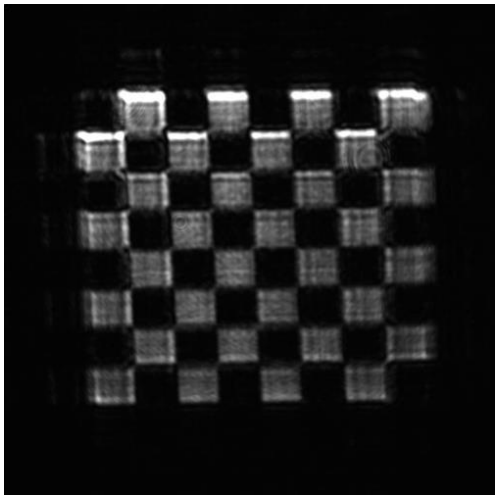

Figure 4.10: (a) Checkerboard Target 256 x 256 image, low pass filtered, and (b) reconstructed holographic image.

A horizontal section of the checkerboard was cropped to view the how well the white and black saturated the image. Fig. 4.11(a) shows the cropped section, and Fig. 4.11(b) reveals the image statistics. Except for the enhanced edge on the left of the picture, the squares are uniformly well filled in.

a)

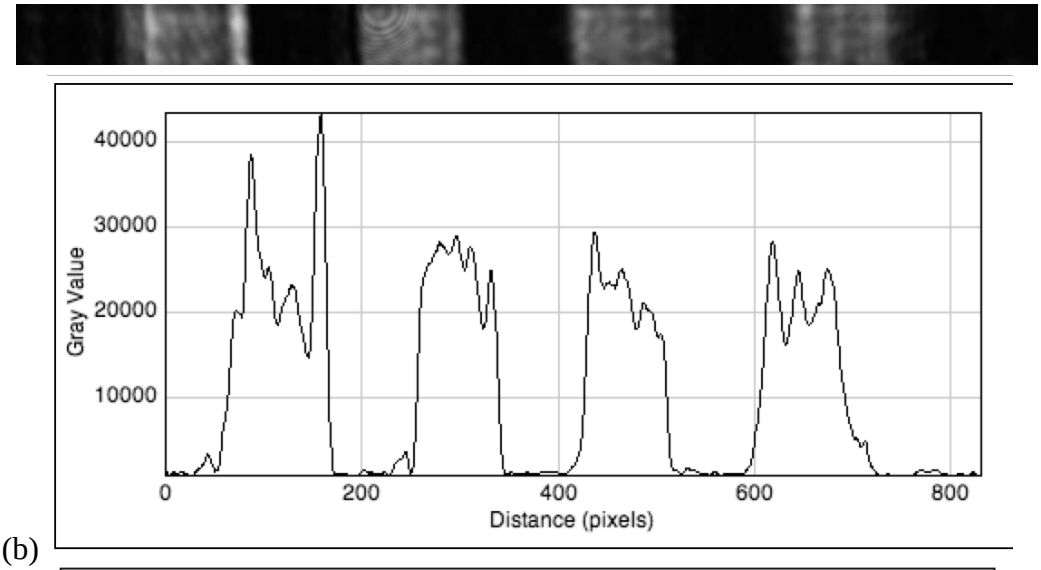

(b)

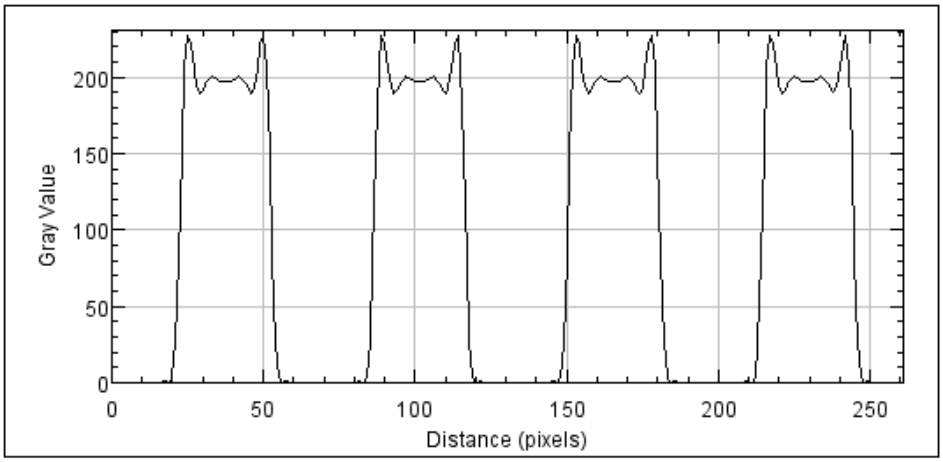

(c)

Figure 4.11: (a) Checkerboard hologram reconstruction section to analyze, (b) gray level plot of section analyzed, and (c) gray level plot of the target image (low pass filtered).

4.6.3 Square Grid

Our last binary image was a square grid of thin bright lines shown in Fig. 4.12. Similar to the checkerboard, fringe effects are visible near the top half, but overall the image can be clearly seen. The lines are of similar width but with some edge light as compared to the target. The blurred portions could be due to minor error in the focus.

(a) 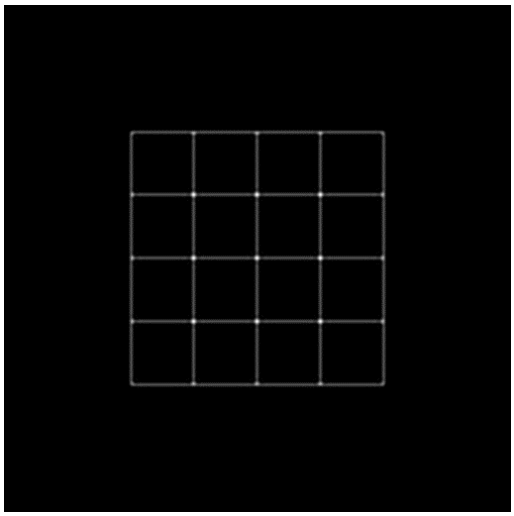 (b) 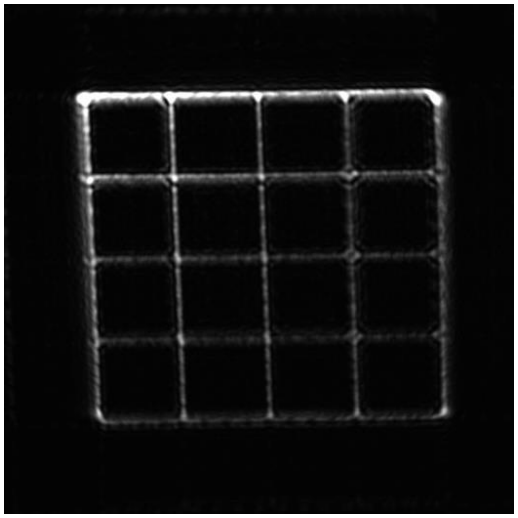

Figure 4.12: (a) Square Grid 256 x 256 Target image, low pass filtered, and (b) reconstructed holographic image.

In addition, a horizontal section of the square grid was cropped to view the white and black saturation. Fig. 4.13(a) shows the cropped section, and Fig. 4.13(b) reveals the image statistics. Reconstructed image had side peaks or fringes that make them look wider or out of focused.

a)

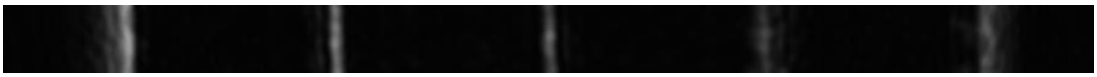

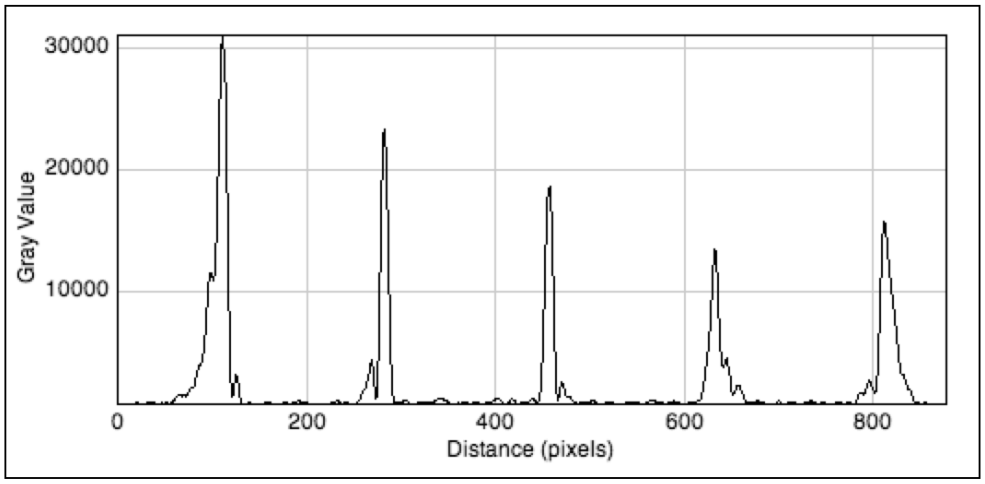

(b)

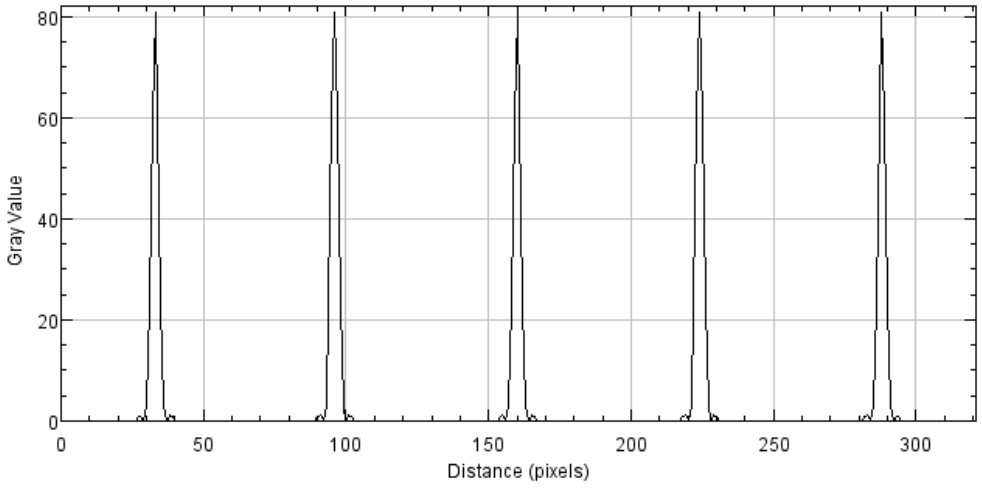

(c)

Figure 4.13: (a) Square grid hologram reconstruction section to analyze, and (b) gray level plot of section analyzed. And (c) gray level plot of the target image (low pass filtered).

4.7 Discussion and Evaluation of Results

In this past chapter, we looked at several holograms and analyzed their reconstruction results. The spatial frequency Air Force resolution chart showed that we could correctly resolve frequencies up to 0.35% of the bandwidth, which is what we specified in Chapter 3.2.5 with low-pass filtering. The gradient pattern revealed that our

complex light modulation technique had trouble reconstructing images with low contrast. The cloth weave like pattern introduced in the grayscale cameraman and Lena images was due to ZOD from the SLM dead space. Images with higher contrast formed better images. Other encoding methods, such as phase-only encoding and iteratively designed G-S encoding, were tested to compare with our complex wavefront reconstruction routine. Phase-only encoding produced a nice contour of the target but lacked much energy, hence the dim output. If the wave amplitude was added to form a complex hologram, it caused light to fill the image in the appropriate areas, and improved the reconstructed image quality. Compared with phase-only holograms of the same image, the fully complex hologram had much better results based on visual comparisons. Compared to the iteratively-designed phase-only Lena hologram, the full-complex hologram contained much less speckle noise.

In summary, we have experimentally demonstrated precise hologram reconstruction using fully complex spatial light modulation. The implementation used the product of separate amplitude and phase modulators. Amplitude modulation was performed by precise beam shaping with a DMD binary modulator and low-pass spatial filter. This output was imaged onto a phase-only SLM creating a fully complex wavefront that reconstructed the desired holographic image.

Chapter 5: Conclusion

5.1 SUMMARY

The complex light modulation method was conceived by Jinyang Liang and Michael Becker as a major progress of their previous research funded by DARPA and the Army Research Office as part of the DARPA Optical Lattice Emulator Initiative (OLE). This thesis examined the experimental implementation of this complex light modulation technique. The goal was to utilize high precision amplitude beam shaping developed by Liang, et. al and pair the technology with off-the-shelf liquid crystal (LC) phase modulation technology to create a high quality hologram. These efforts depended on utilizing a digital micromirror device (DMD) for precise beam shaping in addition to phase modulation using LC technology.

Chapter 1 provided some background for full complex modulation, described various full-complex modulation techniques, and shared an overview of SLM technology. Chapter 2 delved into diffraction theory and address spatial bandwidth limitations. Chapter 3 explained our optical setup and the procedure to make full-complex holograms, ranging from DMD pattern generation to low-pass filtering. Chapter 4 provided an image analysis of each hologram produced and compared the full complex results with phase-only and iterative phase-only hologram designs. Ultimately, we showed how a DMD was used to create the amplitude portion of the hologram and how the LC modulator was used to create the phase portion of the hologram.

5.2 NEXT STEPS

As seen in the previous chapter, the complex hologram reconstruction fidelity depends on several factors such as the astigmatism of the DMD and gray level distortion.

The next steps are to examine the root-mean-square (RMS) error between the phase-only and fully complex holograms and implement various techniques to improve the reconstructed holographic image quality such as ZOD suppression. We plan to compare our full-complex method with additional phase algorithms and complete a numerical analysis using image processing tools, such as the Structural Similarity Index.[26] We also aim to leverage amplitude and phase SLMs in the market that may have higher pixel density and bandwidth.

5.3 APPLICATIONS

We have identified the three potential use cases and applications for complex light modulation. In the *consumer electronics industry*, by incorporating full-complex holograms in virtual reality, the consumer can find new applications in 3-D visualization, gaming, and healthcare. In the *biomedical industry*, CLM may allow for regularly visible light to reveal anatomical structure deep inside the human body. If harmless light can be wave-guided and refocused using the phase and amplitude, then doctors may have an alternative solution to X-ray based imaging methods. The technology may also be able to refocus the light inside the tissue, which enables the non-invasive photo-thermal therapy with high resolution. Third, in the *cybersecurity industry*, security personnel can encrypt or decrypt their data using diffraction patterns. These diffraction patterns can create holograms, when laser-illuminated, in order to reveal hidden security information.

[26] Wang, Zhou, Alan Conrad Bovik, Hamid Rahim Sheikh, and Eero P. Simoncelli. "Image quality assessment: from error visibility to structural similarity." Image Processing, IEEE Transactions on 13.4 (2004): 600-612.

Vita

Vik Parthiban is a Masters student in Electrical Engineering at The University of Texas at Austin. He studies the interaction of Light & Matter, and how one can use holography for new applications such as 3D displays and augmented reality. He completed his undergraduate study at UT in Computer Engineering & Plan II Honors, and writes for the Vector Engineering magazine. Carrying a penchant for design and a passion for innovation, he founded two startups, WiMi Head-up Display and Cramen Spice Blends in graduate school. Besides research and academics, he also teaches Differential Calculus for freshmen and Senior Capstone Design for seniors. In his free time, he enjoys playing violin and spending quality time with people. His projects can be found on his personal website at https://vikparthiban.wordpress.com/about/.

Permanent email: vikparthiban@utexas.edu

This thesis was typed by Vik Parthiban.

References

1. Alexander Jesacher, Christian Maurer, Andreas Schwaighofer, Stefan Bernet, and Monika Ritsch-Marte, "Near-perfect hologram reconstruction with a spatial light modulator," Opt. Express 16, 2597-2603 (2008).
2. C. Slinger, C. Cameron, and M. Stanley. Computer-Generated Holography as a Generic Display Technology. IEEE. 2005.
3. D.E. Smalley, Q.Y.J Smithwick, V.M. Bove Jr., J. Barabas, and S. Jolly. Anisotropic leaky mode modulator for holographic video displays. Nature 498. June, 2013.
4. D. Gabor, "A New Microscopic Principle", Nature, 161, 777, 1948.
5. Gerchberg, R.W. and Saxton, W.O., “A practical algorithm for the de- termination of the phase from image and diffraction plane pictures,” Optik 35, 237–246 (1972).
6. James M. Florence ; Richard D. Juday; Full-complex spatial filtering with a phase mostly DMD. Proc. SPIE 1558, Wave Propagation and Scattering in Varied Media II, 487 (November 11, 1991); doi:10.1117/12.49655.
7. Liang, J., Kohn, R.N., Becker, M.F., and Heinzen, D.J., "1.5% root-mean-square flat-intensity laser beam formed using a binary-amplitude spatial light modulator," Applied Optics vol. 48(10), 1955-1962 (2009).
8. Liang, J., Kohn, R.N., Becker, M.F., and Heinzen, D.J., "High-precision laser beam shaping using a binary-amplitude spatial light modulator,” Applied Optics vol. 49(8), 1323-1330, (2010).
9. Liang, J., Wu, S.-Y., Kohn Jr, R. N., Becker, M. F., and Heinzen, D. J., “Grayscale laser image formation using a programmable binary mask,” Optical Engineering, 51(10), (2012).
10. Liang, J. and Becker, M. F. , “Precise holograms using complex light modulation,” Proc. of SPIE 8979, 89790D-1 to 9 (2014).

11. Luiz Gonçalves Neto, Danny Roberge, and Yunlong Sheng, "Full-range, continuous, complex modulation by the use of two coupled-mode liquid-crystal televisions," Appl. Opt.35, 4567-4576 (1996).
12. "Microsoft HoloLens." Microsoft HoloLens. Microsoft, n.d. Web.
13. "Magic Leap." Magic Leap. N.p., n.d. Web.
14. Ostromoukhov,V., “A simple and efficient error-diffusion algorithm,” Proc. SIGGRAPH 2001, pp. 567–572, ACM, New York, NY (2001).
15. P.A. Blanche, et al. An Updatable Holographic Display for 3D Visualization. Journal of Display Technology, 4. 2008.
16. Wang, Zhou, Alan Conrad Bovik, Hamid Rahim Sheikh, and Eero P. Simoncelli. "Image quality assessment: from error visibility to structural similarity." Image Processing, IEEE Transactions on 13.4 (2004): 600-612.